Korean J. Chem. Eng., 35(7), 1547-1555 (2018)
DOI: 10.1007/s11814-018-0059-z

pISSN: 0256-1115
eISSN: 1975-7220

Electrodeposition-fabricated PtCu-alloy cathode catalysts for high-temperature proton exchange membrane fuel cells

Hyanjoo Park*, Kyung Min Kim, Hoyoung Kim*, Dong-Kwon Kim*, Yong Sun Won**,†, and Soo-Kil Kim*,†**

*School of Integrative Engineering, Chung-Ang University, 84 Heukseokno, Dongjak-gu, Seoul 06974, Korea
**Department of Chemical Engineering, Pukyong National University, 365, Sinseon-ro, Nam-gu, Busan 48547, Korea
(*Received 29 January 2018 • accepted 28 March 2018*)

Abstract−Pt electrocatalysts in high-temperature proton exchange membrane fuel cells (HT-PEMFCs) containing phosphoric acid (PA)-doped polymer membranes are prone to poisoning by leaked PA. We performed a preliminary density functional theory (DFT) study to investigate the relationship between the electronic structure of Pt surfaces and their adsorption of PA. Excess charge on Pt was found to weaken its bonding with the oxygen in PA, thus presenting a strategy for the fabrication of PA-resistant catalyst materials. Consequently, PtCu-alloy catalysts with various compositions were prepared by electrodeposition. The morphologies and crystalline structures of the alloys were strongly dependent on alloy composition. Moreover, the Pt atoms in the PtCu-alloy catalysts were found to be in an electron-rich state, similar to that of the excessively charged Pt simulated in the DFT study. As a result, the oxygen reduction reaction activities of the PtCu-alloy catalysts were superior to that of a Pt-only catalyst, regardless of the presence of PA. In the absence of PA, the higher activity of the PtCu-alloy catalysts was ascribable to conventional alloying effects, while the increased activity in the presence of PA was largely due to the enhanced resistance to PA poisoning. Therefore, PtCu-alloy catalysts easily prepared by electrodeposition were found to be strong candidate materials for HT-PEMFC electrodes.

Keywords: High-temperature PEMFC, Oxygen Reduction Reaction, Phosphoric Acid Poisoning, PtCu-alloy Catalysts, Density Functional Theory (DFT) Study

INTRODUCTION

High-temperature proton exchange membrane fuel cells (HT-PEMFCs), which normally employ phosphoric acid (PA)-doped polybenzimidazole (PBI) membrane [1-4] and operate at temperatures above 100 °C, have the advantages of fast kinetics, enhanced CO tolerance, utilization of wasted heat, and system simplification by the elimination of humidifiers [5-7]. However, such devices are prone to PA leakage from the membrane to the electrode during operation, blocking the active sites of the catalyst and thus reducing the performance of the electrodes [8-10]. Generally, the slow kinetics and consequently high overpotential of the oxygen reduction reaction (ORR) over cathode Pt catalysts limit the performance of PEMFCs [11,12]. In the case of HT-PEMFCs, this performance deterioration is accelerated by PA poisoning [13-15]. Park et al. reported an experimental study on PA poisoning [16], in which the ratio of surface Pt atoms poisoned by PA was determined using extended X-ray absorption fine structure (EXAFS) spectroscopy and cyclic voltammetry (CV). In addition, the coordination number of the Pt was used as an index for the degree of PA adsorption. The authors concluded that the higher coordination number in 0.1 M $HClO_4$+10 mM H_3PO_4 electrolyte, in contrast with the lower coordination number in 0.1 M $HClO_4$, was due to both Pt-OH bond formation and PA adsorption on the Pt surface. Furthermore, He et al. reported the ORR activity of PtNi/C catalysts fabricated by chemical synthesis at various phosphate concentrations [17]. Besides the higher ORR activity of PtNi/C than that of Pt/C in the absence of PA, the PtNi/C catalyst exhibited only a 34-mV shift in half-wave potential, while that for Pt/C was 60 mV. In addition, Chung et al. reported an Ar-annealed PtNi catalyst having an ORR current density of 45% that obtained in the absence of PA [18]. Similar results for the relative ORR activities of PtCo/C alloy and Au_{core}-Pt_{shell} catalysts in the absence and presence of PA have been reported [19].

The strategy for the development of an HT-PEMFC catalyst resistant to PA adsorption can be inferred from the strategies used in the development and improvement of cathode catalysts for low-temperature PEMFCs (LT-PEMFCs). The ORR activity in LT-PEMFCs is greatly affected by the nanostructure of the electrodes, the type and composition of the alloy materials, and the crystal facet of the catalysts [20,21]. For example, the alloys of Pt with 3d transition metals such as Ni, Fe, Cu, or Co show increased catalytic activity owing to both alloying effects and structural effects, such as alteration of the Pt-Pt bond length [22,23] and the coordination number [24,25] and electronic structure of Pt [26-28]. The Pt-transition metal alloys used to catalyze the ORR exhibit increased electron density on Pt upon alloying with transition metals whose atomic size or electronegativity are smaller than those of Pt. This increased electron density promotes the ORR by decreasing the strength of adsorption of the oxygen species on the Pt surface [29], thus weak-

†To whom correspondence should be addressed.
E-mail: yswon@pknu.ac.kr, sookilkim@cau.ac.kr

ening their adsorption. Similarly, the adsorption of PA on Pt surfaces involves bonding between oxygen atoms (in the PA molecule) and Pt. Nart et al. investigated the adsorption of PA on Pt surfaces [30]. According to their study, PA adsorbed on Pt can adopt two different configurations depending on the applied potential; a bidentate structure with two oxygen atoms coordinated to the Pt surface forms at low potential, while a monodentate structure with one oxygen atom coordinated to the Pt surface forms at higher potential owing to the presence of PtOH. It is clear that the adsorption of PA on Pt surfaces depends on bonding between PA oxygen atoms and surface Pt atoms. Therefore, it should be possible to suppress the PA poisoning of Pt electrodes by changing the electronic structure of the Pt in such a way as to weaken its interactions with the oxygen atoms of PA. This may be achieved by the same strategy as that used to weaken the interactions of Pt with the oxygen species involved in the ORR, i.e., alloying with transition metals. This idea is also in accordance with the concept that changes in the d-band center of the catalysts, i.e., lowering, lead to the weak adsorption of anions on Pt surface [31], such as phosphate in this case.

In the present study, the change in the strength of adsorption of PA on Pt was first simulated by a computational method according to the surface charge of Pt. As indicated in the earlier section, the concept of preventing PA adsorption on the catalyst surface by modulating the electronic structure was tried first in this study and the computational simulation provided theoretical validation and support for the concept and guide to the experimental study. Once established, the idea was experimentally verified using PtCu-alloy catalysts fabricated by electrodeposition. Though several studies on PtCu-alloy for ORR applications have been reported [32,33], its effect on the PA adsorption and subsequent function on HT-PEMFC ORR has been rarely investigated. Electron-rich Pt was realized by alloying with Cu, which has lower electronegativity (2.2 vs. 1.9) and a smaller atomic radius (138 vs. 128 pm) than Pt. The electrodeposition method has the advantages of simpler processing, easier control of product composition, lower cost, and higher product purity than those of conventional chemical synthesis. Using the electrodeposition method, PtCu-alloy catalysts with various morphologies and alloy compositions were prepared, and their electrochemical ORR activities were measured in both the absence and presence of PA. The physicochemical properties of the fabricated PtCu-alloy catalysts were thoroughly analyzed using a range of spectroscopic techniques and related with their catalytic activity in the ORR. Despite the numerous studies on PtCu-alloy catalysts for LT-PEMFCs, though, its behavior in the presence of PA for application to HT-PEMFCs has barely been investigated.

EXPERIMENTAL

1. Computational Details

The possibility has been proposed that charge transfer from Cu to Pt in an alloy of Cu_xPt_y would affect the adsorption of PA and its ionic species, such as phosphate ions ($H_2PO_4^-$), onto Pt surface. To validate this presumption, a density functional theory (DFT) study for a simple system where a phosphate ion is located on the Pt (111) surface has been performed. The Pt (111) surface was selected as it is the most distinctive plane in X-ray diffraction (XRD) measurements, and the phosphate ion as a charged adsorbate was used to maximize the binding characteristics. Then, a widely used vacuum slab model [34,35] was introduced to quantify the binding energy between the adsorbate and the metal surface, as shown in Fig. 1. The Pt (111) surface was cleaved from the primitive cell of the bulk face-centered cubic (FCC) structure having a lattice constant of 3.9239 Å [36]. Three layer slabs were built with a sufficiently large vacuum thickness of 20 Å to avoid any effects on the binding energy calculation from the upper and lower slabs. The surface was then expanded by 2×2 to prevent interaction between adsorbates. Therefore, the first (or uppermost) layer was composed of 25 Pt atoms, and the second and third layers comprised 16 atoms each. Meanwhile, the fractional coordinates of all the layers were fixed during changes to the lattice (or during the calculation), although the first layer could be relaxed together with the adsorbate. However, the focus here was to obtain the change of the binding energy with respect to the charge build-up on the Pt surface, and thus the coordinate relaxation would have a limited effect on the trend (or comparison) of the binding energy change. The computation time was the other factor as well.

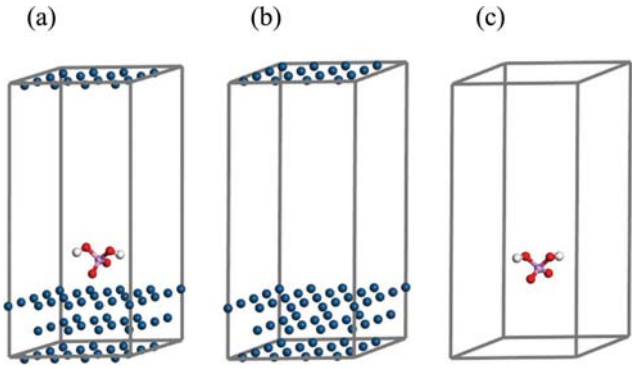

Fig. 1. Scheme of the binding energy calculation in vacuum slab models. $E_{binding}$=E of (a) - E of (b) - E of (c).

The binding energy between the phosphate ion and the Pt (111) surface was simply calculated by the following relationship, also as illustrated in Fig. 1. In short, the energy values should be calculated based on the same supercell. Geometry optimization of the supercell of Pt (111) slabs was not necessary because the fractional coordinates of the layers were fixed during the calculation, as mentioned above.

$E_{binding}$=Energy of the geometry-optimized supercell with $H_2PO_4^-$ on Pt (111) slabs
- Energy of the supercell of Pt (111) slabs
- Energy of the geometry-optimized supercell with $H_2PO_4^-$ only

DFT calculations for geometry optimization and binding energies were carried out using our vacuum slab geometries using the CASTEP program suite [37,38] in Materials Studio (Accelrys Inc., USA). The DFT exchange-correlation potential used in the calculation was the generalized gradient approximation (GGA) along with the PW91 (Perdew-Wang) functional [39]. Core and valence electron interactions were considered using on-the-fly generation (OTFG) ultrasoft pseudopotentials [40] and a plane-wave basis set

with a cutoff energy of 381 eV. The tolerance for energy convergence was set to as low as 5.0×10^{-5} eV/atom to speed up the calculation.

2. Catalyst Preparation and Characterization

PtCu-alloy catalysts were prepared by an electrodeposition method. For the electrodeposition, 0.5 M H_2SO_4 was used as a supporting electrolyte, and the Pt precursor $H_2PtCl_6{\cdot}xH_2O$ at various concentrations ranging from 1 to 30 mM and 5 mM $CuSO_4$ as Cu precursor were added. Furthermore, a Pt-only catalyst was prepared for comparison using 30 mM $H_2PtCl_6{\cdot}xH_2O$ as a metal precursor and 0.5 M H_2SO_4 as a supporting electrolyte. Each electrolyte was purged with N_2 gas for at least 30 min to remove dissolved oxygen from the electrolyte. The Pt-only and PtCu-alloy catalysts were electrodeposited onto glassy carbon rotating disk electrodes (GC RDE, 0.0707 cm^2, Metrohm, for electrochemical analysis) and glassy carbon films (1.6×1.6 cm^2, thickness: 60 μm, Sigradur, for material analysis) to form working electrodes. A Pt plate and a saturated calomel electrode (SCE, saturated KCl) were used as the counter and reference electrodes, respectively. Electrodeposition was performed at room temperature and ambient pressure conditions using a potentiostat (Autolab PGSTAT302N, Metrohm) with a fixed deposition potential of −1.2 V for 60 s. The morphologies of the fabricated Pt-only and PtCu-alloy catalysts were characterized by field-emission scanning electron microscopy (FE-SEM, SIGMA, Carl Zeiss), and the compositions of the PtCu-alloy catalysts were analyzed by energy dispersive X-ray spectroscopy (EDX). Furthermore, the crystal structures were analyzed using XRD (New D8-Adavance, BRUKER-AXS) in an angle range from 30 to 90° at a scan rate of 5°/min. X-ray photoelectron spectroscopy (XPS, ThermoFisher Scientific, K-alpha+) was performed to confirm the electronic structure of Pt in the catalysts. Also, the Pt loading amounts were measured using an inductively coupled plasma mass spectrometer (ICP-MS, MASS, Agilent 7900) to determine the mass activities.

3. Electrochemical Measurements

The catalytic activity of the materials for the ORR was tested using linear-sweep voltammetry (LSV) with a voltage range of 0.05 to 1.05 V (vs. RHE) at scan rate of 10 mV/s. The working electrode was rotated at 1,600 rpm. The electrolyte for the ORR was 0.1 M $HClO_4$ either with or without 0.1 M H_3PO_4, and these solutions were purged with O_2 for at least 1 h before starting the experiment. The roughness factors of the catalysts were measured using CV at a voltage range of 0 to 1.2 V (vs. RHE) and a scan rate of 10 mV/s. The electrolyte was 0.1 M $HClO_4$ either with or without 0.1 M H_3PO_4, and it was purged with Ar for at least 1 h before starting the experiment. All electrochemical experiments were conducted at room temperature and ambient pressure.

RESULTS AND DISCUSSION

1. DFT Calculation

Preliminary DFT calculations were employed to assess the change in the binding energy between phosphate ions and the Pt (111) surfaces according to the charge build-up on the Pt surface. The reference was a phosphate ion located on an uncharged Pt (111) surface, so that the total charge of the vacuum slab system was −1, due to the phosphate ion. Then, it was assumed that charge is transferred from Cu to Pt in an alloy of PtCu, and the charge transfer is proportional to the amount of Cu in the alloy. Thus, charges were considered to be concentrated locally on Pt atoms. DFT calculations were carried out to obtain the binding energies with changes in the total charge of the system. Fig. 2 demonstrates the trend of the binding energy changes with respect to the charge applied to the system. The charge applied to the system (x-axis) is zero for the reference state. When a charge is added to the system (−1 on the x-axis), the total charge of the system becomes −2 (−1 from the added charge and −1 from the phosphate ion). The added charge is distributed between the 57 Pt atoms in the slabs. The result (y-axis) is expressed by $\Delta E_{binding}$ ($E_{binding}$-$E_{binding}$ at the reference point). When five units of charge are removed from the Pt (111) surface, the phosphate ion binds to the surface much more strongly. Conversely, when a unit of charge is applied to the surface, the binding energy of the phosphate ion to the Pt (111) surface decreases by 0.2 eV. The binding energy reaches a plateau at a certain point (−20 applied charges/57 Pt atoms=−0.35 per atom) and drops significantly afterwards. The inset images of the phosphate ions in Fig. 2 also present a certain trend. At the reference point, the non-protonated oxygen of the phosphate ion interacts with a surface Pt atom, forming a monodentate binding conformation [41]. As charges are applied, the non-protonated oxygen retreats from the surface and two oxygen atoms that are not bonded to hydrogen atoms (one non-protonated and one deprotonated oxygen atom) become involved in the adsorption equally, adopting a bidentate binding conformation. When excess charge is added, the structure of the phosphate ion becomes distorted from the surface.

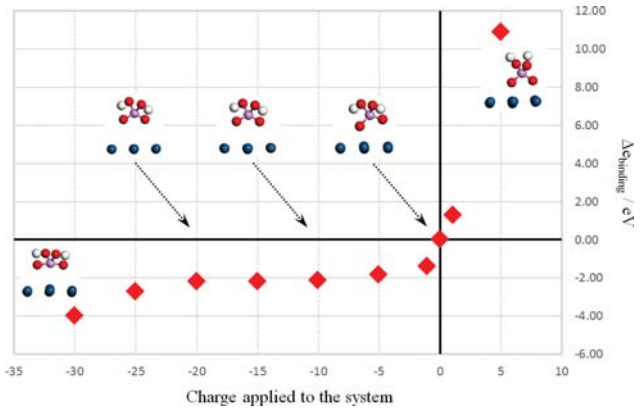

Fig. 2. Binding energy change with respect to the charge applied to the system.

2. Characterization of PtCu-alloy Catalysts

As can be seen from the results of the above calculations, the adsorption of PA on the Pt surface is strongly influenced by the surface charge on the Pt. Since the charge on Pt atoms can be increased by alloying with Cu, the strength of PA adsorption can be thus decreased. To validate this assertion, PtCu-alloy catalysts were fabricated on GC supports by electrodeposition and assessed. The FESEM images and alloy compositions of the prepared catalysts are shown in Fig. 3. In the case of the Pt-only catalyst (Fig. 3(a)), polyhedral particles of ~100-nm size are uniformly electrodeposited on the GC. Fig. 3(b)-(h) shows the surface morpholo-

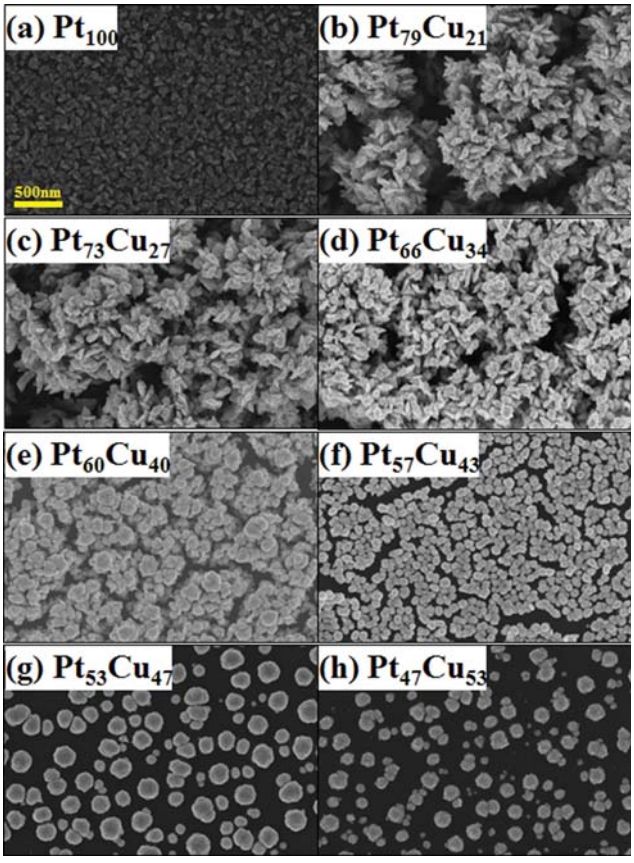

Fig. 3. FESEM images and alloy compositions of Pt-only and PtCu-alloy catalysts electrodeposited at −1.2 V (vs. SCE) for 60 s.

gies and compositions of the PtCu-alloy catalysts as a function of the concentration of the Pt precursor used in their synthesis, which was varied from 1 to 30 mM while the concentration of the Cu precursor was maintained at 5 mM. These catalysts show dramatic morphological change from needle-like to round. The $Pt_{79}Cu_{21}$ catalyst, which has the highest Pt content (Fig. 3(b)) among the PtCu-alloy catalysts, is deposited as an agglomeration of needle-like particles. As the Pt content gradually decreases, more round particles are observed. In case of the $Pt_{47}Cu_{53}$ catalyst (Fig. 3(h)), which has the lowest Pt content (and thus the highest Cu content), 150-nm-sized round particles are electrodeposited on the GC, and the coverage is decreased. There have been many studies on the fabrication of PtCu nanostructures with different shapes depending on their relative Pt and Cu contents [42-45]. Particularly, structures similar to the dendritic forms presented by $Pt_{79}Cu_{21}$ (Fig. 3(b)) and $Pt_{66}Cu_{34}$ (Fig. 3(d)) arising from the controlled kinetic synthesis of Pt_3Cu have been reported [46]. The dramatic changes in the morphologies shown in Fig. 3 cannot be explained by one simple theory. However, it may be related to complex variables such as differences in surface energies and growth rates (the electrodeposition speeds originated from the standard reduction potentials, in this case).

Fig. 4 shows the XRD patterns for the Pt-only and PtCu-alloy catalysts. The fabricated Pt has a polycrystalline FCC structure, and Pt (111), (200), (220), and (311) peaks are observed at 39.76°, 46.24°, 67.45°, and 81.28°, respectively (JCPDS 04-0802). Peaks corresponding to Cu (111), (200), and (220) are 43.29°, 50.43°, and 74.13°, respectively (JCPDS 04-0836), and marked in the figure. As can be seen from Fig. 4, the Pt peaks of the PtCu-alloy catalysts are positively shifted as compared with those of the Pt-only catalyst. As the Cu content increases, the peaks are more positively shifted owing to the decrease in the lattice constant of Pt upon alloying. This lattice contraction is one of the main reasons that Pt-based alloy catalysts exhibit improved ORR activities [47,48].

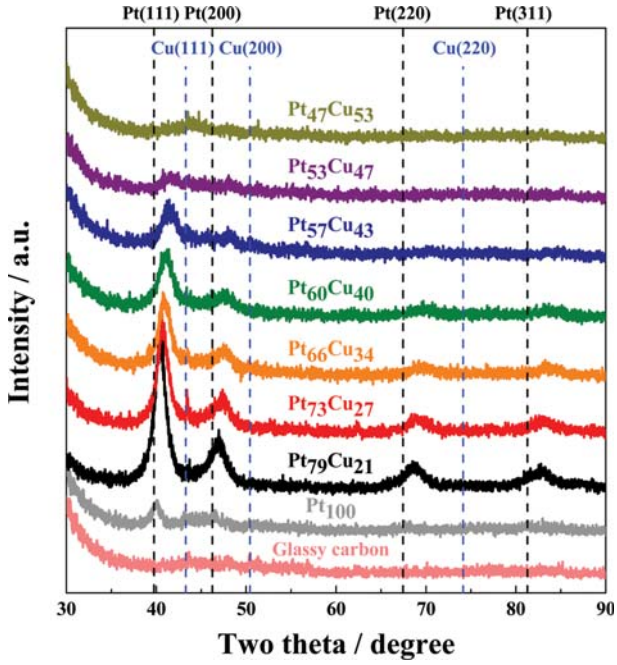

Fig. 4. XRD results for the Pt-only and PtCu-alloy catalysts.

The electronic structure of the PtCu-alloy catalysts was analyzed by XPS. Fig. 5(a) shows the Pt $4f_{5/2}$ and Pt $4f_{7/2}$ peaks for the Pt-only and PtCu-alloy catalysts. For the PtCu-alloy catalysts, the Pt 4f peak is negatively shifted as the content of Cu increases. The reason for this shift is the electron transfer from Cu to Pt, which occurs owing to the difference in electronegativity between Pt (2.28) and Cu (1.90). Fig. 5(b) shows the Cu $2p_{1/2}$ and Cu $2p_{3/2}$ peaks of the PtCu-alloy catalysts. The binding energies of the Cu 2p electrons increase as the Pt content increases. The Cu 2p binding energy for the $Pt_{79}Cu_{21}$ catalyst, which has the lowest Cu content, is the highest, indicating a decrease in electron density upon electron transfer from Cu to Pt. In addition, because Cu has a smaller atomic size than that of Pt, the alloying of the two metals causes changes in the lattice constant. The core-level shift does not directly reflect the shift of d-band center. However, these changes in the electronic structure are closely related to the weakening of the binding of oxygenated species to Pt, affecting the ORR activity [49-52]. In addition, since the adsorption of PA on Pt occurs through Pt-O bonds (similarly to the adsorption of oxygenated species during the ORR), modification of the electronic structure of Pt by Cu alloying can also weaken the adsorption of PA anion. This can also be deduced from the result of the DFT simulation shown in Fig. 2. Thus, modification of the electronic structure of Pt by alloy-

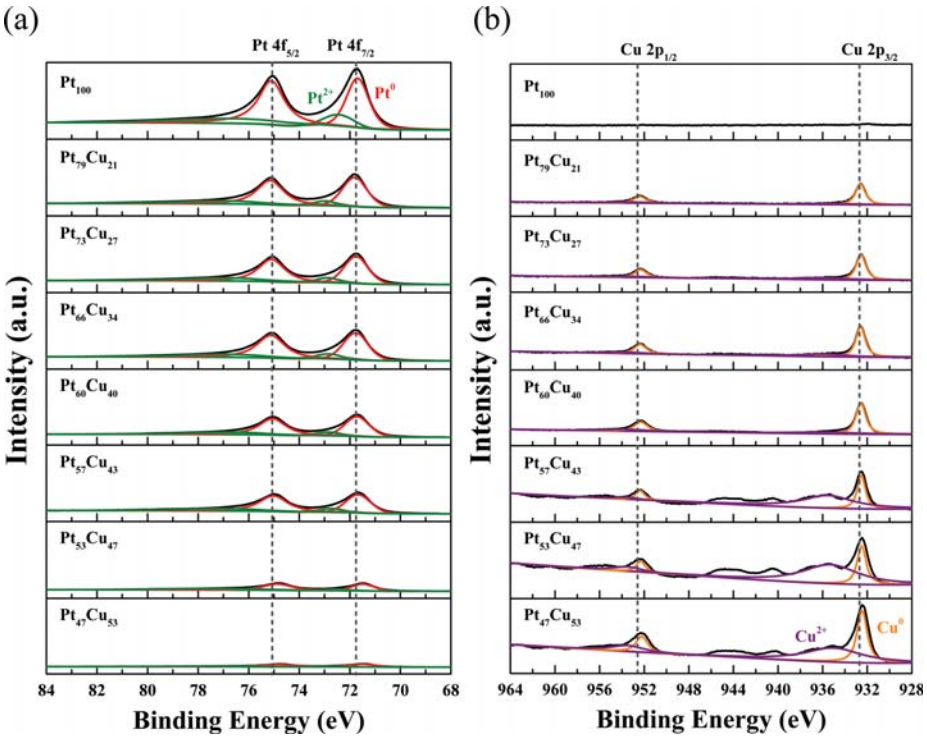

Fig. 5. (a) Pt 4f and (b) Cu 2p XPS spectra of PtCu-alloy catalysts compared with those of the Pt-only catalyst.

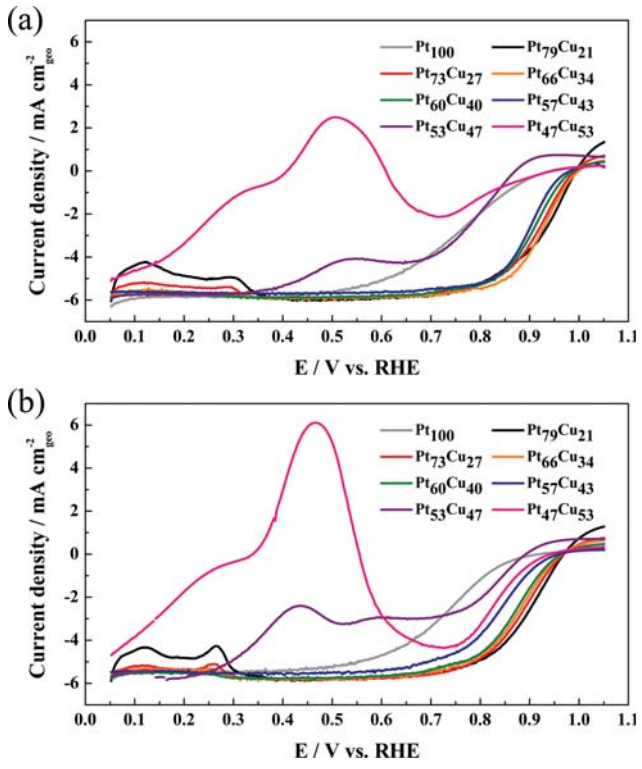

Fig. 6. ORR polarization curves for the Pt-only and PtCu-alloy catalysts in O_2-saturated 0.1 M $HClO_4$ electrolyte (a) in the absence and (b) in the presence of PA. Linear sweep voltammetry measurements were performed from 0.05 to 1.05 V (vs. RHE) at a scan rate of 10 mV s^{-1} and 1,600 rpm at room temperature.

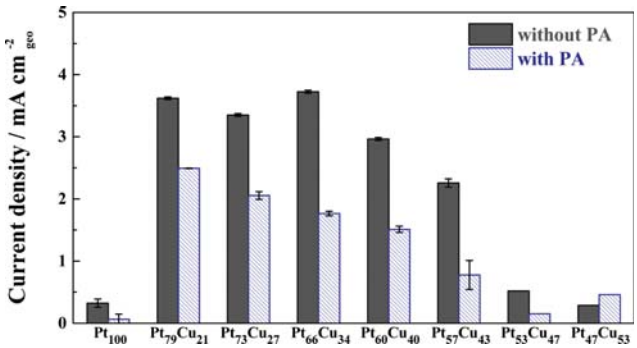

Fig. 7. Comparison of the ORR activities of the Pt-only and PtCu-alloy catalysts based on the current densities at 0.9 V (vs. RHE) presented in Fig. 6.

ing with Cu is effective for both the enhancement of ORR activity and suppression of PA adsorption.

3. ORR Activity of PtCu-alloy Catalysts

Fig. 6 shows the polarization curves for the ORR over the Pt-only and PtCu-alloy catalysts in O_2-saturated 0.1 M $HClO_4$ electrolyte in the absence (Fig. 6(a)) and presence (Fig. 6(b)) of PA. The $Pt_{47}Cu_{53}$ and $Pt_{53}Cu_{47}$ catalysts, which have Cu content close to 50%, do not exhibit typical ORR behavior, regardless of the presence of PA. The peaks observed around 0.5 V are due to the competition between the anodic current of Cu dissolution and the limiting current of the ORR. However, the PtCu-alloy catalysts having Cu content of 21-43% exhibit better ORR activities than that of the Pt-only catalyst, regardless of the presence of PA, and these activities are strongly correlated with the composition of the alloy.

Note that He el al. reported that peaks associated with the adsorption of "weakly-bonded" hydrogen and "strongly-bonded" hydrogen in the hydrogen underpotential deposition (UPD) region were clearly observed at 0.13 and 0.26 V, respectively [17], and the same peaks were obtained in Fig. 6 as well.

For more precise comparisons of the ORR activities according to the presence of PA and the composition of the alloys, the current densities at 0.9 V (vs. RHE) obtained from Fig. 6 were plot-

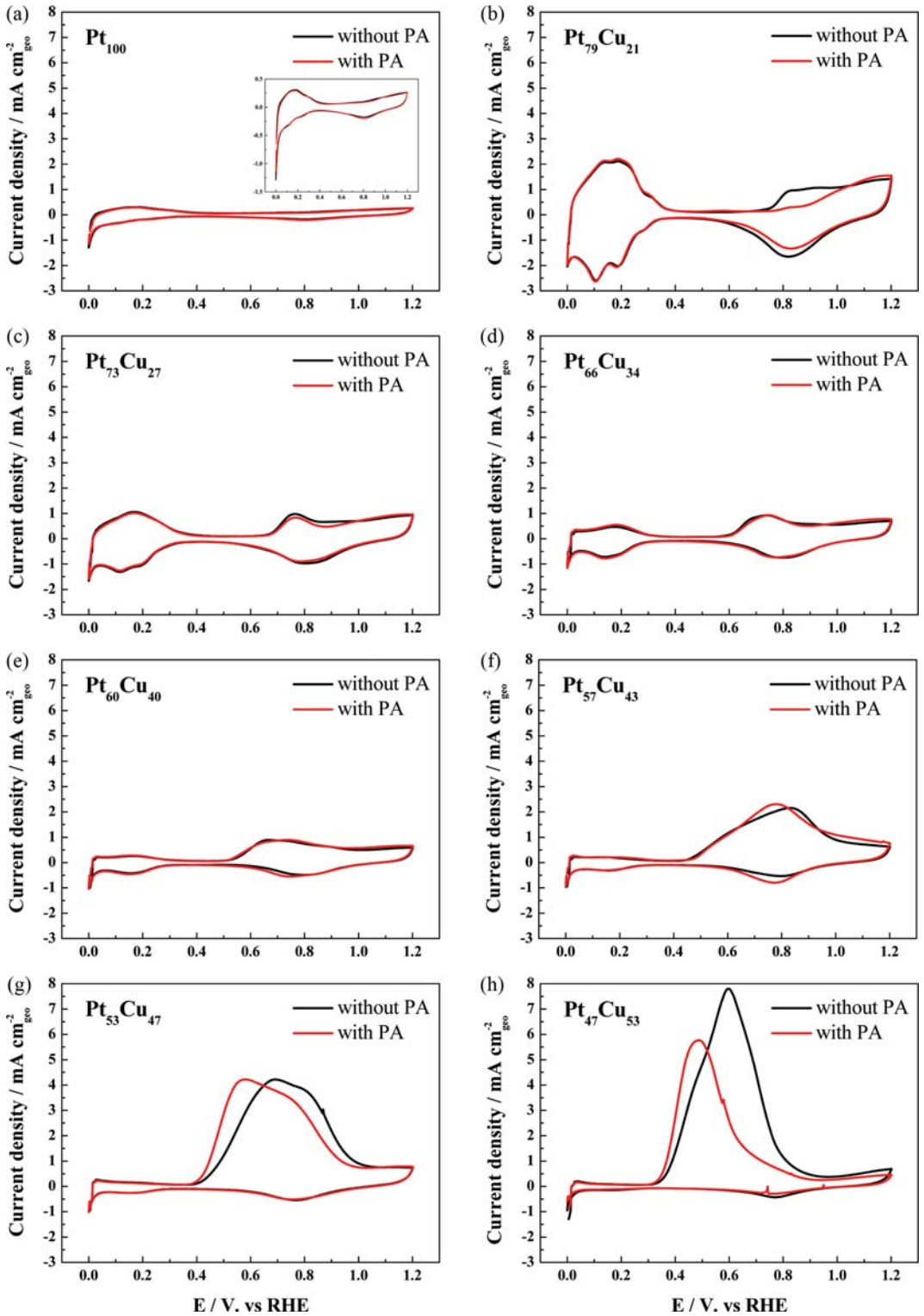

Fig. 8. Cyclic voltammograms (CV) of the Pt-only and PtCu-alloy catalysts in Ar saturated 0.1 M $HClO_4$ electrolyte in the absence (black line) and presence (red line) of PA. CV was performed from 0 to 1.2 V (vs. RHE) at a scan rate of 10 mV s^{-1} at room temperature.

ted, as shown in Fig. 7. All the PtCu-alloy catalysts except for the $Pt_{53}Cu_{47}$ and $Pt_{47}Cu_{53}$ catalysts show significantly better ORR activities than that of the Pt-only catalyst in the absence of PA, and the $Pt_{66}Cu_{34}$ catalyst exhibits a maximum current density 11-times higher than that of the Pt-only catalyst. Besides the electronic and structural effects of Cu alloying described earlier, the OH_{ads} inhibition effect might play an important role in this case. According to Su et al., the preferentially orientated (111) and (110) planes of PtCu-alloy catalysts in $HClO_4$ electrolyte are less vulnerable to OH_{ads} than the (100) plane, thereby improving catalytic activity [53]. As shown in the XRD results (Fig. 4), the PtCu-alloy catalysts (except the $Pt_{53}Cu_{47}$ and $Pt_{47}Cu_{53}$ catalysts) have better developed (111) and (220) planes than those of the Pt-only catalyst. For the comparison of obtained ORR activity with literatures (in the absence of PA), the highest ORR current density of 3.72 mA cm^{-2} at 0.9 V was obtained in the case of $Pt_{66}Cu_{34}$ catalyst. This is higher than most of reported PtCu-alloy catalysts such as PtCu NTs catalyst (2.50 mA cm^{-2}) [53], PtCu/NPG catalyst (3.7 mA cm^{-2}) [54], PtCu/C catalyst (2.5 mA cm^{-2}) [55], or comparable with $Pt_{62}Cu_{38}$ core-shell BNAFs catalyst (4.1 mA cm^{-2}) [56].

However, in the presence of PA, the PtCu-alloy catalysts (except those with the highest Cu contents) show decreased ORR activity owing to phosphate poisoning while still maintaining higher activity than that of the Pt-only catalyst. For the $Pt_{79}Cu_{21}$ catalyst, which exhibits the highest ORR activity in the presence of PA, the current density at 0.9 V (vs. RHE) in the presence of PA is ~2.50 mA cm^{-2}, which was ~38.4-times higher than that of the Pt-only catalyst in the presence of PA (0.065 mA cm^{-2}). This means that the increment in current density upon alloying with Cu is much larger in the presence of PA (0.065 to 2.50 mA cm^{-2}, a 38-fold increase) than in the absence of PA (0.32 to 3.60 mA cm^{-2}, an 11-fold increase). This implies that i) the PtCu-alloy catalysts have better ORR activity than that of the Pt-only catalyst regardless of the presence of PA, and ii) the alloying not only improves ORR activity but also mitigates PA poisoning by weakening the adsorption of PA on Pt. Note that the activity of $Pt_{79}Cu_{21}$ catalyst (2.49 mA cm^{-2} at 0.9 V) is higher than $Pt_{69}Au_{31}$ catalyst (0.1 mA cm^{-2}) [15] or comparable to Au_{core}-Pt_{shell}/C catalyst (2.8 mA cm^{-2}) [19].

To evaluate the morphological effect on ORR performance for the PtCu-alloy catalysts, CV analysis of the Pt-only and PtCu-alloy catalysts according to the presence of PA was performed, and the results are shown in Fig. 8. For the Pt-only catalyst (Fig. 8(a)), peaks corresponding to hydrogen adsorption and desorption are weakly observed between 0.0 to 0.3 V (vs. RHE) (inset). However, for $Pt_{79}Cu_{21}$-$Pt_{66}Cu_{34}$ shown in Fig. 8(b)-(d), the area for proton adsorption and desorption (0.0 to 0.3 V vs. RHE) is dramatically increased proportionally with the Pt/Cu ratio. This is largely due to the highly hierarchical structures shown in Fig. 3. As the composition ratio decreases (Fig. 8(e)-(h)), the proton-related area gradually decreases, as can be reasonably explained by the morphological changes in Fig. 3. In addition, with increased Cu content (i.e., Cu content over 40%), the redox couple of PtOH formation and reduction with a peak potential at ~0.8 V overlaps with Cu dissolution occurring in the lower potential region around 0.6 to 0.8 V, and this overlapped peak area is dominated by Cu dissolution at the much higher Cu content of 47 and 53%.

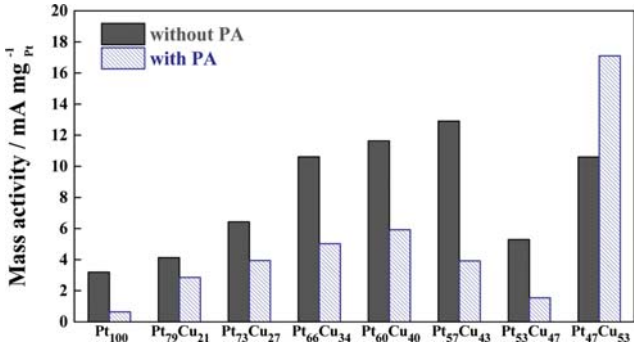

Fig. 9. Comparison of the mass activities of the Pt-only and PtCu-alloy catalysts at 0.9 V (vs. RHE).

From the proton-related peaks in Fig. 8, the roughness factors (RFs) for each catalyst were calculated. In the case of the Pt-only catalyst, the RF value is 26.22 in the absence of PA. However, in the case of the PtCu-alloy catalysts in Fig. 8(b)-(h), the RF values are 212.5, 98.1, 38.48, 20.23, 13.79, 12.73, and 4.87, respectively. The RF of the $Pt_{79}Cu_{21}$ catalyst is 8.1-times higher than that of the Pt-only catalyst owing to the dendritic growth of $Pt_{79}Cu_{21}$ particles (Fig. 3), which contribute partially to higher performance.

Fig. 9 compares the mass activity of the Pt-only and PtCu-alloy catalysts obtained from the ICP-MS analysis and current density at 0.9 V (vs. RHE). Note that the mass activity of the $Pt_{53}Cu_{47}$ and $Pt_{47}Cu_{53}$ catalysts has no significant meaning due to the severe interference by Cu dissolution, as shown in Fig. 6. The Pt-only catalyst exhibits relatively low mass activity compared to those of the PtCu-alloy catalysts, regardless of the presence of PA. In the absence of PA, the $Pt_{57}Cu_{43}$ catalyst exhibits ~4-times higher mass activity than that of the Pt-only catalyst (12.9 vs. 3.20 mA/mg_{Pt}). In the presence of PA, however, the $Pt_{60}Cu_{40}$ catalyst exhibits the highest mass activity of 5.93 mA/mg_{Pt}, which is ~9.3-times higher than that of the Pt-only catalyst. The deterioration of mass activity for the Pt-only catalyst by PA poisoning is ~80.0%, while that for $Pt_{60}Cu_{40}$ is only 49.1%, demonstrating the resistance of PtCu-alloy catalysts to PA poisoning. Therefore, it is concluded that PtCu-alloy catalysts are promising candidates for cathode materials for HT-PEMFCs containing PA-doped membranes.

CONCLUSIONS

PtCu-alloy catalysts were assessed as cathode materials resistant to PA poisoning for application in HT-PEMFCs. DFT calculations indicated that excess charge on Pt weakens the strength of PA adsorption on Pt surfaces. Subsequently, PtCu-alloy catalysts with various compositions were prepared by electrodeposition. The fabricated PtCu-alloy catalysts with Cu content from 20-40% exhibited needle-like morphologies, which are in part beneficial to catalytic activity, while the Pt-only and other PtCu-alloy catalysts presented round particles. XRD and XPS analysis confirmed the formation of alloys with electron-rich Pt through charge transfer from Cu to Pt, which provided a similar environment to the excess charge on Pt simulated in the DFT calculations. In the absence of PA, the ORR activities of the prepared PtCu-alloy catalysts presented a

maximum current density 11-times higher than that of the Pt-only catalyst. Though there was still deterioration in the ORR activities of the PtCu-alloy catalysts when PA was present in the electrolyte, the deterioration rate was much smaller than that of the Pt-only catalyst, and the PtCu-alloy catalysts exhibited ~38-times higher current density than that of the Pt-only catalyst. Furthermore, the mass activity of the PtCu-alloy catalysts was significantly higher than that of the Pt-only catalyst. Therefore, it was confirmed that PtCu-alloy catalysts with various compositions can be easily prepared by electrodeposition, and are strong candidate materials for HT-PEMFC electrodes.

ACKNOWLEDGEMENT

This work was supported by the National Research Foundation of Korea (NRF) Grant funded by the Korean Government MSIT (grant number 2016M1A2A2937146) and Korea CCS R&D Center (KCRC) (grant number 2014M1A8A1049349).

REFERENCES

1. M. Moradi, A. Moheb, M. Javanbakht and K. Hooshyari, *Int. J. Hydrogen Energy*, **41**, 2896 (2016).
2. E. Quartarone and P. Mustarelli, *Energy Environ. Sci.*, **5**, 6436 (2012).
3. S. S. Araya, F. Zhou, V. Liso, S. L. Sahlin, J. R. Vang, S. Thomas, X. Gao, C. Jeppesen and S. K. Kær, *Int. J. Hydrogen Energy*, **41**, 21310 (2016).
4. Y. Ma, A. Schechter, J. S. Wainright and R. F. Savinell, *J. Electrochem. Soc.*, **151**, A8 (2004).
5. A. Chandan, M. Hattenberger, A. El-kharouf, S. Du, A. Dhir, V. Self, B. G. Pollet, A. Ingram and W. Bujalski, *J. Power Sources*, **231**, 264 (2013).
6. E. Quartarone, S. Angioni and P. Mustarelli, *Materials*, **10**, 687 (2017).
7. Y. Liu, W. Lehnert, H. Janßen, R. C. Samsun and D. Stolten, *J. Power Sources*, **311**, 91 (2016).
8. H.-Y. Park, D.-H. Lim, S. J. Yoo, H.-J. Kim, D. Henkensmeier, J. Y. Kim, H. C. Ham and J. H. Jang, *Scientific Reports*, **7**, 7186 (2017).
9. J. B. Floriano, E. A. Ticianelli and E. R. Gonzalez, *J. Electroanal. Chem.*, **367**, 157 (1994).
10. R. Gisbert, G. García and M. T. M. Koper, *Electrochim. Acta*, **55**, 7961 (2010).
11. K. Li, Y. Li, Y. Wang, F. He, M. Jiao, H. Tang and Z. Wu, *J. Mater. Chem. A*, **3**, 11444 (2015).
12. J. Chlistunoff and B. Pivovar, *J. Electrochem. Soc.*, **162**, F890 (2015).
13. D.-C. Jeong, B. Mun, H. Lee, S. J. Hwang, S. J. Yoo, E. Cho, Y. Lee and C. Song, *RSC Adv.*, **6**, 60749 (2016).
14. E. Heider, N. Ignatiev, L. Jörissen, A. Wenda and R. Zeis, *Electrochem. Commun.*, **48**, 24 (2014).
15. J.-E. Lim, U. J. Lee, S. H. Ahn, E. Cho, H.-J. Kim, J. H. Jang, H. Son and S.-K. Kim, *Appl. Catal. B: Environ.*, **165**, 495 (2015).
16. H.-Y. Park, S. H. Ahn, S.-K. Kim, H.-J. Kim, D. Henkensmeier, J. Y. Kim, S. J. Yoo and J. H. Jang, *J. Electrochem. Soc.*, **163**, F210 (2016).
17. Q. He, B. Shyam, M. Nishijima, D. Ramaker and S. Mukerjee, *J. Phys. Chem. C*, **117**, 4877 (2013).
18. Y.-H. Chung, S. J. Kim, D. Y. Chung, M. J. Lee, J. H. Jang and Y.-E. Sung, *Phys. Chem. Chem. Phys.*, **16**, 13726 (2014).
19. K.-S. Lee, S. J. Yoo, D. Ahn, S.-K. Kim, S. J. Hwang, Y.-E. Sung, H.-J. Kim, E. Cho, D. Henkensmeier, T.-H. Lim and J. H. Jang, *Electrochim. Acta*, **56**, 8802 (2011).
20. E. Antolini, *Appl. Catal. B: Environ.*, **217**, 201 (2017).
21. C. Cui, L. Gan, H.-H. Li, S.-H. Yu, M. Heggen and P. Strasser, *Nano Lett.*, **12**, 5885 (2012).
22. M.-k. Min, J. Cho, K. Cho and H. Kim, *Electrochim. Acta*, **45**, 4211 (2000).
23. H. Yang, W. Vogel, C. Lamy and N. Alonso-Vante, *J. Phys. Chem. B*, **108**, 11024 (2004).
24. G. G. Asara, L. O. Paz-Borbón and F. Baletto, *ACS Catal.*, **6**, 4388 (2016).
25. F. Calle-Vallejo, J. Tymoczko, V. Colic, Q. H. Vu, M. D. Pohl, K. Morgenstern, D. Loffreda, P. Sautet, W. Schuhmann and A. S. Bandarenka, *Science*, **350**, 185 (2015).
26. Z. Yang, S. Pedireddy, H. K. Lee, Y. Liu, W. W. Tjiu, I. Y. Phang and X. Y. Ling, *Chem. Mater.*, **28**, 5080 (2016).
27. V. Stamenkovic, B. S. Mun, K. J. J. Mayrhofer, P. N. Ross, N. M. Markovic, J. Rossmeisl, J. Greeley and J. K. Nørskov, *Angew. Chem. Int. Ed.*, **45**, 2897 (2006).
28. Y. Zhao, J. Liu, Y. Zhao, F. Wang and Y. Song, *J. Mater. Chem. A*, **3**, 20086 (2015).
29. Y.-F. Huang and M. T. M. Koper, *J. Phys. Chem. Lett.*, **8**, 1152 (2017).
30. F. C. Nart and T. Iwasita, *Electrochim. Acta*, **31**, 385 (1992).
31. Y.-H. Chung, D. Y. Chung, N. Jung and Y.-E. Sung, *J. Phys. Chem. Lett.*, **4**, 1304 (2013).
32. M. Wang, W. Zhang, J. Wang, A. Minett, V. Lo, H. Liu and J. Chen, *J. Mater. Chem. A*, **1**, 2391 (2013).
33. C. Xu, H. Zhang, Q. Hao and H. Duan, *ChemPlusChem*, **79**, 107 (2014).
34. I. S. P. Savizi and M. J. Janik, *Electrochim. Acta*, **56**, 3996 (2011).
35. E. Skúlason, G. S. Karlberg, J. Rossmeisl, T. Bligaard, J. Greeley, H. Jónsson and J. K. Nørskov, *Phys. Chem. Chem. Phys.*, **9**, 3241 (2007).
36. S. M. Foiles, M. I. Baskes and M. S. Daw, *Phys. Rev. B*, **33**, 7983 (1986).
37. M. C. Payne, M. P. Teter, D. C. Allan, T. A. Arias and J. D. Joannopoulos, *Rev. Mod. Phys.*, **64**, 1045 (1992).
38. M. D. Segall, P. J. D. Lindan, M. J. Probert, C. J. Pickard, P. J. Hasnip, S. J. Clark and M. C. Payne, *J. Phys.: Condens. Matter*, **14**, 2717 (2002).
39. J. P. Perdew, J. A. Chevary, S. H. Vosko, K. A. Jackson, M. R. Pederson, D. J. Singh and C. Fiolhais, *Phys. Rev. B*, **46**, 6671 (1992).
40. D. Vanderbilt, *Phys. Rev. B*, **41**, 7982 (1990).
41. R. Zeis, Beilstein, *J. Nanotechnol.*, **6**, 68 (2015).
42. D. Xu, Z. Liu, H. Yang, Q. Liu, J. Zhang, J. Fang, S. Zou and K. Sun, *Angew. Chem. Int. Ed.*, **48**, 4217 (2009).
43. B. Y. Xia, H. B. Wu, X. Wang and X. W. Lou, *J. Am. Chem. Soc.*, **134**, 13934 (2012).
44. J. Ding, X. Zhu, L. Bu, J. Yao, J. Guo, S. Guo and X. Huang, *Chem. Commun.*, **51**, 9722 (2015).
45. S. Chen, H. Su, Y. Wang, W. Wu and J. Zeng, *Angew. Chem. Int. Ed.*, **54**, 108 (2015).
46. E. Taylor, S. Chen, J. Tao, L. Wu, Y. Zhu and J. Chen, *ChemSusChem*, **6**, 1863 (2013).

47. W. Yang, L. Zou, Q. Huang, Z. Zou, Y. Hu and H. Yang, *J. Electrochem. Soc.*, **164**, H331 (2017).
48. W. Xiao, M. A. L. Cordeiro, M. Gong, L. Han, J. Wang, C. Bian, J. Zhu, H. L. Xinb and D. Wang, *J. Mater. Chem. A*, **5**, 9867 (2017).
49. S. J. Yoo, S. J. Hwang, J.-G. Lee, S.-C. Lee, T.-H. Lim, Y.-E. Sung, A. Wieckowskid and S.-K. Kim, *Energy Environ. Sci.*, **5**, 7521 (2012).
50. B. Hammer, Y. Morikawa and J. K. Nørskov, *Phys. Rev. Lett.*, **76**, 2141 (1996).
51. V. Stamenkovic, B. S. Mun, K. J. J. Mayrhofer, P. N. Ross, N. M. Markovic, J. Rossmeisl, J. Greeley and J. K. Nørskov, *Angew. Chem.*, **118**, 2963 (2006).
52. A. Ruban, B. Hammer, P. Stoltze, H. L. Skriver and J. K. Nørskov, *J. Mol. Catal. A: Chem.*, **115**, 421 (1997).
53. L. Su, S. Shrestha, Z. Zhang, W. Mustaina and Y. Lei, *J. Mater. Chem. A*, **1**, 12293 (2013).
54. H. Zhang, B. Yi, Y. Zeng, S. Jiang, Y. Jiang, Y. Bai and Z. Shao, *RSC Adv.*, **6**, 40086 (2016).
55. L. Cao, G. Zhang, W. Lu, X. Qin, Z. Shao and B. Yi, *RSC Adv.*, **6**, 39993 (2016).
56. S. Fu, C. Zhu, Q. Shi, D. Du and Y. Lin, *Catal. Sci. Technol.*, **6**, 5052 (2016).